Effects of chemical order and atomic relaxation on the electronic and magnetic properties of $La_{2/3}Sr_{1/3}MnO_3$



2009 J. Phys.: Condens. Matter 21 115602

(http://iopscience.iop.org/0953-8984/21/11/115602)

J. Phys.: Condens. Matter **21** (2009) 115602 (9pp) doi:10.1088/0953-8984/21/11/115602

# Effects of chemical order and atomic relaxation on the electronic and magnetic properties of $La_{2/3}Sr_{1/3}MnO_3$

**B Zheng**[1,2,3] **and N Binggeli**[1,4]

[1] Abdus Salam International Centre for Theoretical Physics, Strada Costiera 11, I-34014 Trieste, Italy
[2] Sincrotrone Trieste, Area Science Park, I-34012 Basovizza, Trieste, Italy
[3] Department of Materials Science and Engineering, Jilin University, Changchun 130021, People's Republic of China
[4] INFM-CNR Democritos National Simulation Center, Miramare, Trieste, Italy

E-mail: zhengb@ictp.it

Received 10 November 2008, in final form 19 January 2009
Published 20 February 2009
Online at stacks.iop.org/JPhysCM/21/115602

**Abstract**

We investigate the effects of Sr/La cation ordering/disordering and atomic relaxation on the electronic and magnetic properties of $La_{2/3}Sr_{1/3}MnO_3$ (LSMO) by means of *ab initio* pseudopotential calculations. We consider a cation-ordered layered structure and a more homogeneously Sr-bulk-doped structure. Cation disordering and atomic relaxation both tend to push the LSMO system towards half-metallicity, increasing the minority-spin and spin-flip gaps. Lattice relaxation has a significant effect on the electronic density of states (DOS) of the layered LSMO and drastically reduces the initial differences found comparing the electronic properties of the perovskite structures with different dopant configurations. The trend with structural relaxation is understood in terms of an effective screening, due to the displacement of the O anions and La cations, of the local electric field produced by the ordered Sr dopants.

(Some figures in this article are in colour only in the electronic version)

## 1. Introduction

The hole-doped lanthanum manganites with the chemical formula $La_{1-x}A_xMnO_3$ (A = Ca, Sr or Ba) exhibit a large variety of electronic and magnetic phases, due to a complex interplay between spin, charge and orbital degrees of freedom of the mixed-valence Mn cations [1, 2]. For $x \approx 1/3$, these systems display negative colossal magnetoresistance near the Curie temperature, $T_C$, and half- or near-half-metallicity below $T_C$ [3–5]. Among these compounds, and for an optimal doping $x \approx 1/3$, $La_{2/3}Sr_{1/3}MnO_3$ (LSMO) exhibits the largest Curie temperature ($T_C \sim 370$ K) and a high spin polarization, which make this system an attractive candidate for current injection in spintronic devices [6], such as magnetic tunneling junctions (MTJs) [7].

The tunneling magnetoresistance (TMR) ratio in LSMO/$SrTiO_3$/LSMO MTJs was found to be more than 1800% at 4 K, from which a spin polarization of at least 95% was inferred for LSMO [8]. The intrinsic half-metal character of LSMO at low temperature, however, is still under debate. Some recent experimental analyses suggest that LSMO is a transport half-metal, rather than a conventional half-metal with no minority electrons at the Fermi level [9]. Other experimental interpretations favor, instead, true half-metallicity for LSMO [10]. *Ab initio* density-functional calculations generally find LSMO to be on the borderline for half-metallicity [11], whereas the inclusion of an ad hoc $U$ of a few eVs within the local density approximation plus on-site Coulomb interaction (LDA + $U$) approach yields a half-metal [12] with a significant spin-flip gap [5]. Despite the very encouraging TMR results reported for LSMO-based MTJ at low temperature, the TMR response was found to decrease much faster than expected with temperature—possibly due to the deterioration of the spin state at the interface [13]. In this context, much current research is being devoted to understanding and controlling the LSMO material [11, 14], defects [15, 16], surface [17, 18] and interface [13, 19, 20] properties.

 

Epitaxial growth techniques, such as molecular-beam epitaxy, are powerful techniques to engineer bulk and interface properties of electronic materials. Recently, such techniques have been applied to perovskite manganese oxides, making possible the fabrication of nanoscaled heterostructures and of heterojunctions with selected-layer termination at the interface [21]. Such techniques are potentially interesting to control the TMR in MTJs by means of interfacial engineering. They can also be used to stabilize new layered perovskite phases, such as cation-ordered epitaxial phases [22, 23], unattainable in bulk materials. In view of their inherent anisotropy, such artificially ordered layered perovskites may exhibit systematic differences in their electronic and magnetic structure with respect to their bulk-alloy counterpart. For example, in the case of the artificial layered $La_{2/3}Ca_{1/3}MnO_3$ system, corresponding to an $(LaMnO_3)_2/(SrMnO_3)_1(001)$ superlattice with a period of two unit-cell layers of $LaMnO_3$ and one unit-cell layer of $SrMnO_3$, a 20% decrease in $T_C$ was reported with respect to the solid–solution alloy [22].

Theoretically, the $(LaMnO_3)_2/(SrMnO_3)_1(001)$ superlattice or 'layered' LSMO structure has been used, for convenience, as a model in atomistic supercell computations to examine the bulk properties of LSMO [11, 24]. Atomic relaxation effects were neglected, however, in such studies. This, together with the use of different density-functional methods or different treatments for the alloy compared to the ordered structure, hinders a direct comparison with calculations performed for the alloy, so as to quantitatively assess and understand the influence of cation ordering/disordering on the bulk properties. Calculations explicitly addressing the bulk-alloy phase have been carried out either by treating the doping by the addition, in $LaMnO_3$, of the desired hole concentration plus a compensating homogeneous negative background [25] or by using the virtual crystal approximation, i.e. by replacing the Sr and La atoms by a virtual atom having the weighted-average valence of $Sr_{1/3}La_{2/3}$ [26, 27].

Comparing, for example, results obtained within the generalized gradient approximation (GGA) both for the layered LSMO [11] and for the alloy LSMO [25], one observes significant differences between the density of states (DOS) in the two cases. First of all, the system is found to be truly half-metallic in the alloy case, in [25] (pseudopotential calculations) with a spin-flip gap [5] larger than 0.3 eV, whereas this is not the case for the layered structure in [11] (full-potential linearized augmented plane-wave calculations), where the Fermi energy is located within the minority-spin $t_{2g}$ band, about 0.3 eV above the bottom of this band. Furthermore, the minority-spin gap is significantly increased (by more than 0.5 eV) for the alloy system, in [25], and the main O-related features are also much sharper compared to the layered structure, in [11]: the latter differences were observed also in local density approximation (LDA) calculations for the layered $(LaMnO_3)_2/(CaMnO_3)_1(001)$ and for the virtual crystal $La_{2/3}Ca_{1/3}MnO_3$ [27, 28]. It is unclear, however, how much of these differences are due to the neglect of lattice relaxation and/or to the use of different calculational schemes and how much is instead truly the effect of the cation ordering/disordering.

Here we investigate the effects of both cation ordering/disordering and lattice relaxation on the electronic and magnetic properties of LSMO. We employ the same calculational scheme for configurations with different degrees of cation order/disorder, namely the GGA pseudopotential method and real atoms—as opposed to virtual atoms—in a large supercell. We consider the layered LSMO as well as a more homogeneously doped LSMO structure. Atomic relaxation and cation disordering are found to induce the same trend, namely they both push the system towards half-metallicity, increasing the minority-spin and spin-flip gaps. Lattice relaxation induces substantial changes in the electronic DOS of the layered LSMO and drastically reduces the differences between the DOS of the two perovskite LSMO structures with different dopant configurations. Although, quantitatively, the differences between the two relaxed atomic structures are small, the more-homogeneously-doped system is found to be half-metallic, within the GGA approach, while the layered structure is not. The lattice-relaxation effects on the electronic structure are explained in terms of an effective screening, generated by the displacement of the O anions and La cations, of the local electric field generated by the dopant distribution.

We would like to stress that the purpose of this paper is to address and understand microscopically the trends in the chemical order/disorder and atomic relaxation effects on the electronic and magnetic properties of LSMO and related systems. The issue of whether LSMO is actually a true half-metal or not is beyond the scope of this paper, as this depends, for example, on the choice of the exchange–correlation functional used. Settling this issue will eventually rely on an experimental demonstration—although calculations may provide some hints.

## 2. Methodology and configurations

The *ab initio* calculations were performed within the density-functional-theory framework using the spin-polarized Perdew–Burke–Ernzerhof [29] exchange–correlation functional. We used the PWSCF code [30] with ultrasoft pseudopotentials [31][5]. The nonlinear-core correction to the exchange–correlation potential was included for La, Mn and Sr. We used a kinetic-energy cutoff of 30 Ryd for the plane-wave expansion of the electronic wavefunctions and of 350 Ryd for the electronic charge density. The calculation of the equilibrium lattice parameters of the layered LSMO structure was performed using a 15-atom tetragonal unit cell (triple perovskite cell along [001]). All other computations were carried out with a 45-atom tetragonal supercell (see figure 1), containing nine formula units of $La_{2/3}Sr_{1/3}MnO_3$ (tripling the perovskite unit cell along [001] and [010]). The tilting of the $MnO_6$ octahedra—which is small in $La_{1-x}Sr_xMnO_3$ for $x > 0.2$ [24, 35]—was neglected.

In the self-consistent-field (SCF) calculations, the Brillouin-zone sampling was performed using a $12 \times 4 \times 4$

[5] The semicore 5s and 5p states of La and 4s and 4p states of Sr were treated as valence states (the pseudopotentials were generated using the reference atomic configurations $3d^5 4s^2 4p^0$ for Mn, $5s^2 5p^6 5d^1 6s^{1.5} 6p^{0.5}$ for La, $4s^2 4p^6 4d^1 5s^1 5p^0$ for Sr and $2s^2 2p^4$ for O). The transferability of Vanderbilt pseudopotentials has been discussed, for example, in [32], with applications to the properties of oxides (see also, e.g., [33] and [34]).

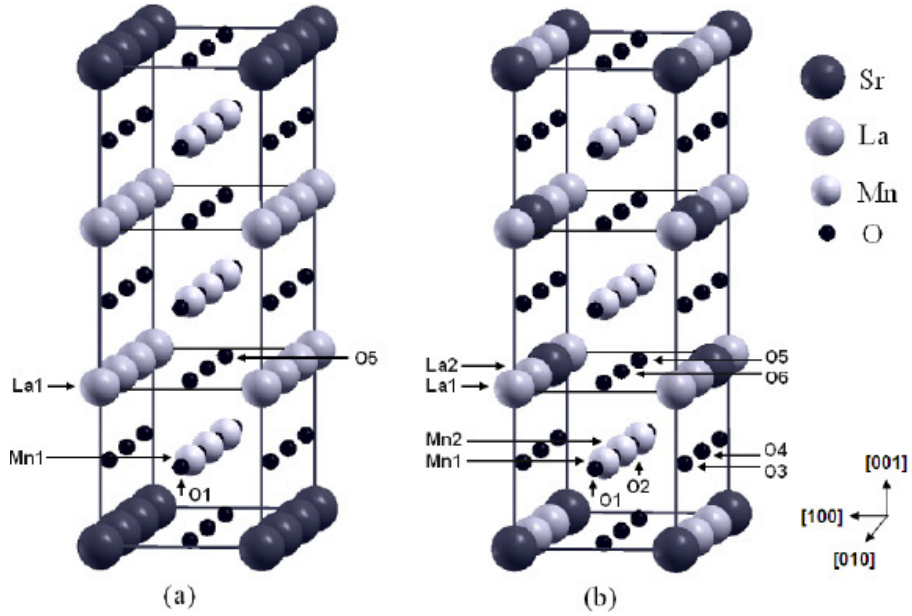


**Figure 1.** Sr-dopant configurations considered in this work for LSMO: (a) the 'layered' configuration (structure A) and (b) a more homogeneous Sr-bulk-doped configuration (structure B). The supercell corresponds to the thick rods, whereas the thin rods highlight the La/Sr(001) cation layers within the supercell—the vertical axis corresponds to the [001] crystallographic direction (or $c$ axis of the layered structure). Large black, large gray, small gray and small black spheres denote Sr, La, Mn and O atoms, respectively. Some representative atoms are labeled for the discussion of the atomic relaxation.

**Table 1.** Atomic relaxations in the layered structure (structure A) and in the more-homogeneously-doped structure (structure B) of LSMO. The atomic relaxations, $\Delta z$ and $\Delta y$, are measured with respect to the ideal cubic perovskite crystal structure with the same lattice parameter $a = 3.88$ Å. The representative atoms and reference axes are labeled according to figure 1.

| | $La_1$ | $La_2$ | $Mn_1$ | $Mn_2$ | $O_1$ | $O_2$ | $O_3$ | $O_4$ | $O_5$ | $O_6$ |
|---|---|---|---|---|---|---|---|---|---|---|
| Structure A | | | | | | | | | | |
| $\Delta z$ (Å) | −0.05 | | −0.01 | | 0.14 | | | | 0.03 | |
| Structure B | | | | | | | | | | |
| $\Delta z$ (Å) | −0.03 | 0.03 | 0.00 | 0.00 | 0.08 | −0.08 | 0.05 | −0.05 | 0.01 | −0.01 |
| $\Delta y$ (Å) | 0.03 | −0.03 | 0.00 | 0.00 | −0.01 | 0.01 | −0.05 | 0.05 | −0.08 | 0.08 |

$k$-point grid centered at Γ for the 45-atom supercell—or equivalently using a 12 × 12 × 4 grid for the 15-atom cell—and we employed a Gaussian level smearing of 0.01 Ryd to determine the Fermi energy. For the DOS calculations, we used a 24 × 8 × 8 $k$-point grid centered at Γ together with the tetrahedron method. Increasing the grid size to 24 × 8 × 8, for the SCF calculations, and to 48 × 16 × 16, for DOS calculations, was found to have a negligible influence on the results reported here. A ferromagnetic alignment of Mn spins was considered in all cases. In the relaxation of the internal atomic structure, the relaxation process was stopped when the forces on the atoms were smaller than 0.001 Ryd/au.

The two different Sr-dopant arrangements considered in this work for LSMO are displayed in figure 1 (unrelaxed configurations). The first configuration, structure A, is the layered structure (figure 1(a)). Starting from a cubic perovskite $LaMnO_3$ system, every third layer of La(001) in this structure has been replaced by a full layer of Sr dopants. The second configuration, structure B, has a more homogeneous Sr-bulk-doped configuration (figure 1(b)). In this structure, one-third of the La atoms in each La(001) layer have been replaced by Sr atoms and all La/Sr(001) atomic planes are equivalent.

## 3. *Ab initio* results

### 3.1. Equilibrium atomic structures

From a series of total energy calculations performed for the layered structure with fully relaxed internal atomic structures at different volumes and, for each volume, at different $c/a$, we obtain the following equilibrium lattice parameters: $a = 3.878$ Å, $c/a = 1.004$, together with a bulk modulus of $B_0 = 156$ GPa. The cell shape is thus virtually cubic and the corresponding lattice parameter is very close to the experimental value $a_{exp} = 3.874$ Å [36]. The calculated bulk modulus is also in reasonable agreement with the experimental value of ∼168 GPa, measured at room temperature [37]. For structure B, considering a cubic cell, we obtain a very similar value of the equilibrium lattice parameter: $a = 3.876$ Å. We thus elected to perform all subsequent calculations using a cubic cell with lattice parameter $a = 3.88$ Å, both for the A and B structures of LSMO.

In table 1, we present the results for the relaxed atomic configuration in the two structures. The largest atomic displacements are observed in the layered structure for O ions

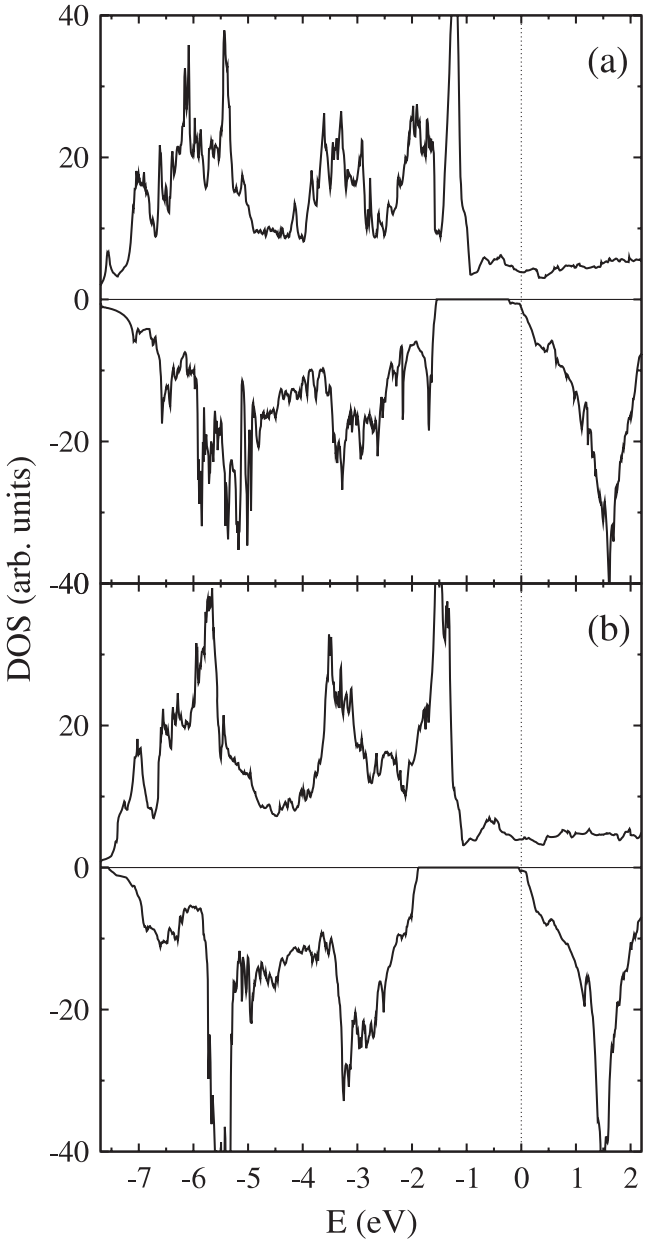


**Figure 2.** Spin-resolved density of states of the layered LSMO (structure A) calculated for the unrelaxed (panel (a)) and relaxed (panel (b)) atomic configurations. The upper (lower) half of each panel corresponds to the majority (minority-) spin states. The dotted line indicates the Fermi energy.

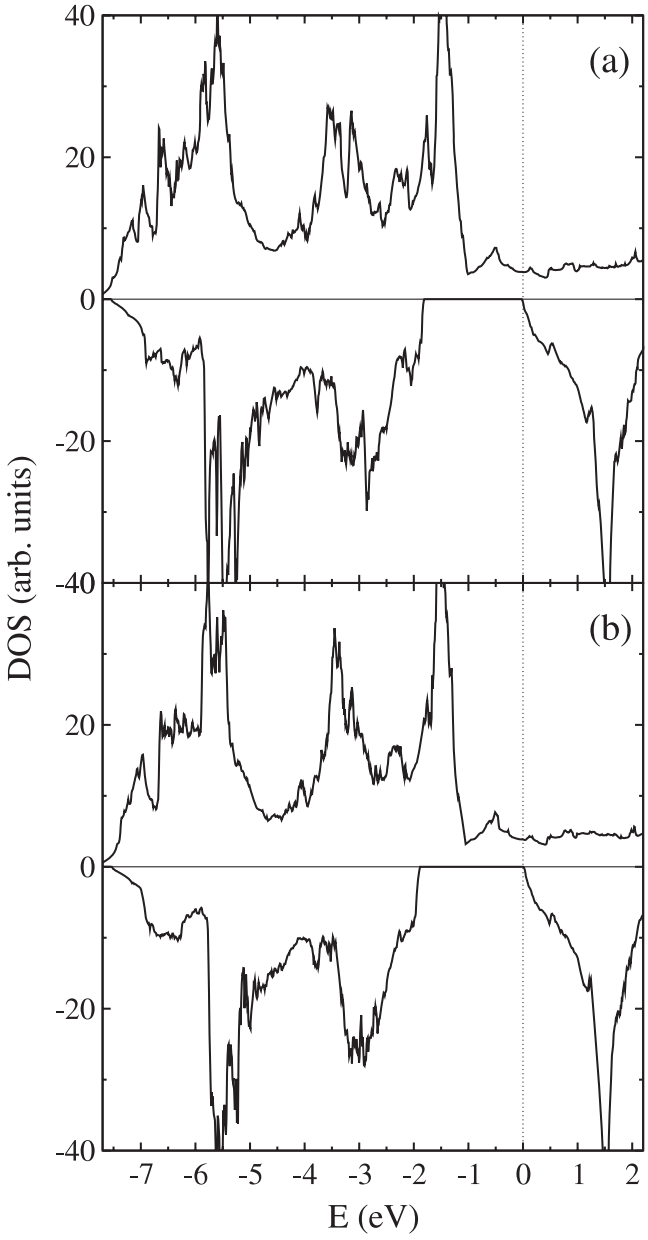


**Figure 3.** The same data as in figure 2, but for the more-homogeneously-doped LSMO (structure B).

located in between the La and Sr planes ($O_1$ ions in table 1 and figure 1(a)). These $O_1$ ions move towards the La plane by 0.14 Å; the La ions in turn move toward the $O_1$ plane by 0.05 Å, so that the resulting O–La (O–Sr) interplanar distance decreases (increases) by 0.19 Å (0.14 Å), which is a significant relaxation. We note that, for the $La_{2/3}Ca_{1/3}MnO_3$ layered perovskite, Pickett and Singh [27] also reported a sizeable relaxation of 0.09 Å for the $O_1$ ions. In structure B, because of the more homogeneous doping, only a buckling of the corresponding O and La(001) layers can take place, and the amplitude of the atomic displacements along [001] is reduced to 0.05–0.08 Å for the O ions and to 0.03 Å for the La ions. Displacements of similar amplitudes also take place along [010]. In structure A (B), the gain in energy due to atomic relaxation is 0.14 (0.07) eV per LSMO formula unit. The relaxed structures A and B are found to be degenerate in energy, within[6] 1 meV/atom—i.e. within the theoretical uncertainty of the *ab initio* calculations.

### *3.2. Electronic and magnetic properties*

In figure 2, we display the spin-resolved DOS of the layered structure A for the unrelaxed (panel (a)) and relaxed

[6] Experimentally, the stable structure is the solid–solution alloy (the A-site cation disordered structure). However, the layered structure synthesized, in the case of $La_{2/3}Ca_{1/3}MnO_3$, by epitaxial growth techniques persists as a metastable phase up to temperatures well above room temperature (for kinetic reasons).

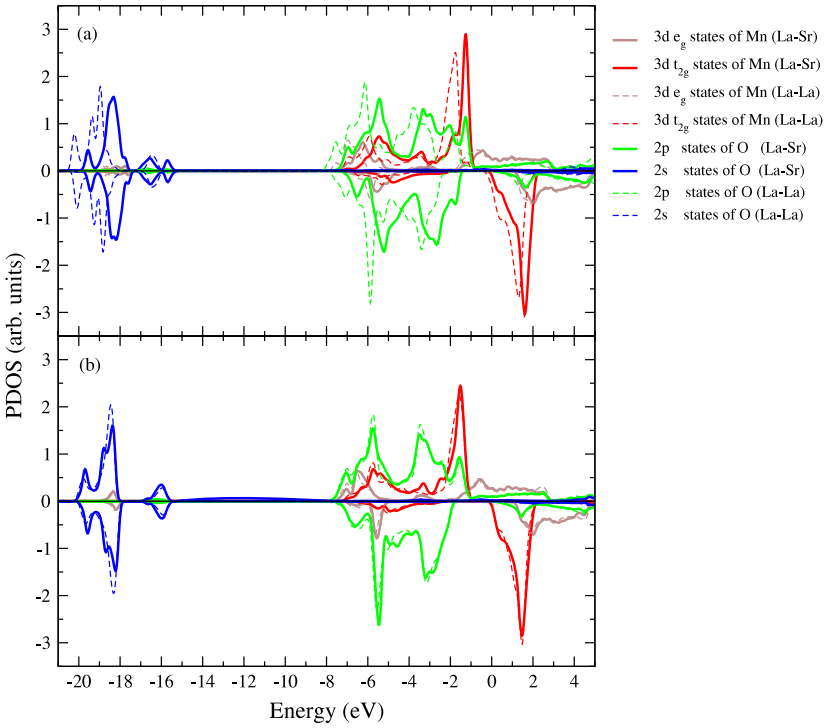


**Figure 4.** Atomic projected density of states (PDOS) of the layered LSMO structure (structure A), calculated for the unrelaxed (panel (a)) and relaxed (panel (b)) atomic configurations. The upper (lower) half of each panel corresponds to the majority (minority) spin states. The zero of energy corresponds to the Fermi level.

(panel (b)) atomic configurations. The zero of the energy scale corresponds to the Fermi energy, $E_F$. The DOS of the relaxed and unrelaxed structures show qualitatively similar main features, which are also generally consistent with previous LDA/GGA calculations [11]. In both cases, a small but finite DOS is present at $E_F$ in the minority-spin channel, showing that the system is not truly half-metallic—although in the relaxed case it is nearly half-metallic. The Mn 3d $t_{2g}$ states give rise to two sharp, characteristic, exchange-split features located at about $-1.5$ eV in the majority-spin DOS and at about $+1.5$ eV in the minority-spin DOS. The majority-spin DOS around $E_F$ has a relatively smooth behavior in the energy window $[-0.8$ eV, $+0.8$ eV$]$, corresponding to Mn 3d-$e_g$ states hybridized with O 2p states, while the minority-spin DOS displays a 1–2 eV bandgap around $E_F$, between occupied O 2p states and Mn $t_{2g}$ states.

Quantitatively there are some noticeable differences, however, between the relaxed and unrelaxed cases. The minority-spin gap, in particular, increases by 0.57 eV with atomic relaxation, i.e. from 1.30 eV in the unrelaxed case to 1.87 eV in the relaxed system. Furthermore, the bottom of the $t_{2g}$ minority-spin band, located at $-0.22$ eV in the unrelaxed structure, is shifted to $-0.04$ eV in the relaxed system. One also observes a significant sharpening of the main O-related DOS features, in particular the features around $-5.5$ and $-3.5$ eV.

Consistent with the shift to higher energy with atomic relaxation of the $t_{2g}$ minority-spin states near $E_F$, the LSMO magnetic moment slightly increases from 3.63 $\mu_B$/Mn (unrelaxed) to 3.66 $\mu_B$/Mn (relaxed)—a value which is close to the measured Mn magnetic moment in LSMO: $\mu_{Mn}^{exp} = 3.7\ \mu_B$ [38]. The canonical value of the LSMO magnetic moment for a fully half-metallic structure is 3.67 $\mu_B$/Mn [28]. The spin polarization, $P = [N_\uparrow(E_F) - N_\downarrow(E_F)]/[N_\uparrow(E_F) + N_\downarrow(E_F)]$, where $N_{\uparrow(\downarrow)}(E_F)$ is the majority-(minority-) spin DOS at $E_F$ [5], also increases from 52% (unrelaxed) to 75% (relaxed). Hence, atomic relaxation increases the tendency towards half-metallicity in the layered structure.

In figure 3, we display the DOS results for the more homogeneously doped structure B, in the unrelaxed (panel (a)) and relaxed (panel (b)) atomic configurations. Structural relaxation induces much smaller changes in the DOS of structure B, compared to structure A. The minority-spin gap increases from 1.80 (unrelaxed) to 1.90 eV (relaxed). The O main peaks around $-5.5$ and $-3.5$ eV, which are already nearly as sharp in the unrelaxed structure B as in the relaxed structure A, become only slightly sharper with relaxation. The bottom of the $t_{2g}$ minority-spin band is located only 0.01 eV below $E_F$ in the unrelaxed structure B and is shifted to 0.02 eV above $E_F$ in the relaxed configuration. The relaxed structure B is hence formally a half-metal, with no minority-spin state at $E_F$.

The magnetic moment also slightly increases from 3.65 $\mu_B$/Mn in the unrelaxed structure B to the canonical value of 3.67 $\mu_B$/Mn in the relaxed structure—a value which is consistent with the experimental value ($\mu_{Mn}^{exp} = 3.7\ \mu_B$ [38]). The spin polarization ratios are 84% and 100% in the unrelaxed and relaxed structures, respectively. Although, quantitatively, relaxation effects are small in structure B, they nevertheless push the system towards half-metallicity. Hence, atomic relaxation and an increased homogeneity in the doping both

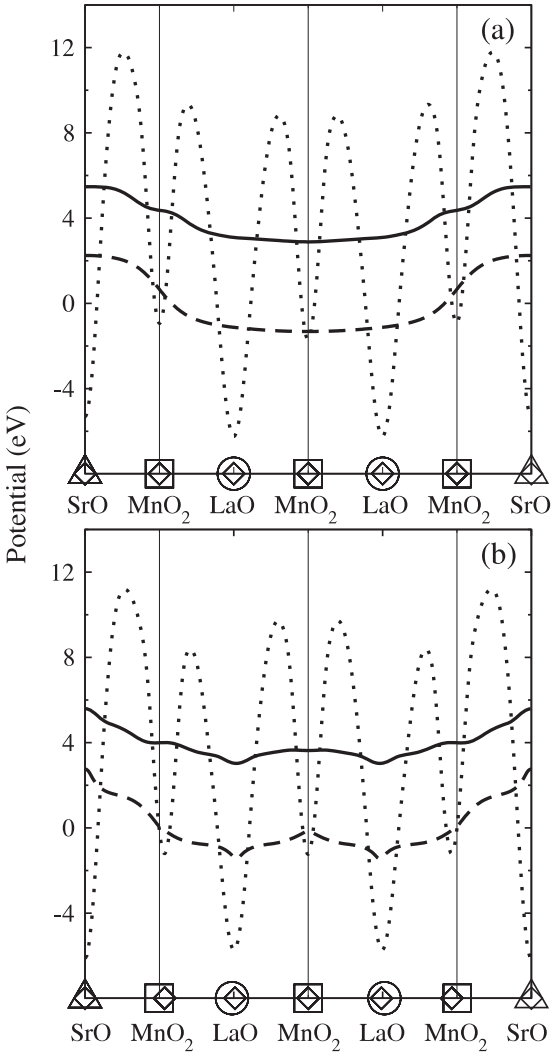


**Figure 5.** Macroscopic averages of the electronic local potential (solid line) and electrostatic potential (dashed line) in the layered perovskite LSMO along the [001] direction for the unrelaxed (panel (a)) and relaxed (panel (b)) atomic configurations. The planar average of the local potential is also shown (dotted line). The atomic layer positions are indicated at the bottom of each panel with the following symbols: ○(circle) La; △(triangle) Sr; □(square) Mn; ◇(diamond) O.

act in the same direction, namely they push the system towards half-metallicity (or make the half-metallic character of the system more robust). Another striking feature is that, except for the small changes around the Fermi energy, the DOS of the relaxed structure A and B are remarkably similar in figures 2(b) and 3(b)—contrary to the case of the unrelaxed structure A and B.

## 4. Discussion of the trends and microscopic interpretation

In order to understand microscopically why the DOS of the structures A and B become so strikingly similar upon structural relaxation, we have examined the behavior of the atomic projected DOS (PDOS) and of the electrostatic potential in the unrelaxed and relaxed structures. In the case of the layered structure, one may distinguish between two different types of $MnO_2(001)$ planes, namely the $MnO_2$ planes which are sandwiched between $Sr^{2+}$–$La^{3+}$ layers and those which are sandwiched between $La^{3+}$–$La^{3+}$ layers (see figure 1(a)). In figure 4, we show the atomic PDOS of the layered structure A for the Mn and O atoms belonging to these two different (La–La-and La–Sr-sandwiched) planes.

In the unrelaxed case (figure 4(a)), one observes that the PDOSs corresponding to Mn and O atoms in the La–La-sandwiched plane are systematically lower in energy with respect to those of the Mn and O atoms in the La–Sr-sandwiched plane[7]—one may also notice that the energy shift increases for orbitals with increased localization (Mn-$t_{2g}$ compared to Mn-$e_g$). A similar shift was also observed earlier for the Mn-$t_{2g}$ states in the layered $La_{2/3}Ca_{1/3}MnO_3$ system [27, 28]. Upon structure relaxation, however, the atomic PDOS features for the two different planes shift in energy towards each other, namely towards their center of gravity, and become essentially degenerate in energy, with PDOS features almost superimposed in figure 4(b).

This trend upon structural relaxation accounts for the increase in the minority-spin and spin-flip gaps and for the sharpening of the O features in figure 2. It can be understood based on the behavior of the electrostatic potential in the LSMO structures. We define the electrostatic potential as the sum of the electronic Hartree potential and ion-point-charge potentials. We also consider a related quantity, the local potential, defined as the sum of the Hartree potential and local part of the pseudopotentials. These two potentials, electrostatic and local, include the same long-range Coulomb-potential component induced by the electrons' and ions' charge distributions, and differ only in the short-range component of the potential.

In figure 5, we display the macroscopic averages [39] of the electrostatic potential and of the local potential in the layered structure A, along the [001] direction. Results are shown both for the unrelaxed (panel (a)) and relaxed (panel (b)) configurations. The macroscopic average is a technique commonly used to study interface band alignments in *ab initio* calculations of semiconductor heterojunctions and superlattices [39]. This technique filters out the sharp atomic-like oscillations present in the SCF potentials, allowing a precise determination of the potential lineups, band offsets and Schottky barrier values [39]. Here we apply this technique to the investigation of the potential profile within the $(LaMnO_3)_2/(SrMnO_3)_1(001)$ superlattice. The macroscopic average $\overline{\overline{V}}(z)$ of a potential $V(x, y, z)$ is the result of two different atomic-scale averaging procedures. The potential is first averaged in the $(x, y)$ plane to yield a planar-averaged potential: $\overline{V}(z) = (1/S)\int_S V(x, y, z)\,\mathrm{d}x\,\mathrm{d}y$, where $S$ is the (001) surface unit cell—the planar average of the local potential $\overline{V}_{\mathrm{loc}}(z)$ is reported in figure 5. At each $z$ position, the macroscopic average of the potential is then obtained by

[7] The minute features located at −17 and −16 eV reflect a small overlap between O 2s states and La 5p states (with energy ∼−17 eV) and Sr 4p states (with energy ∼−16 eV).

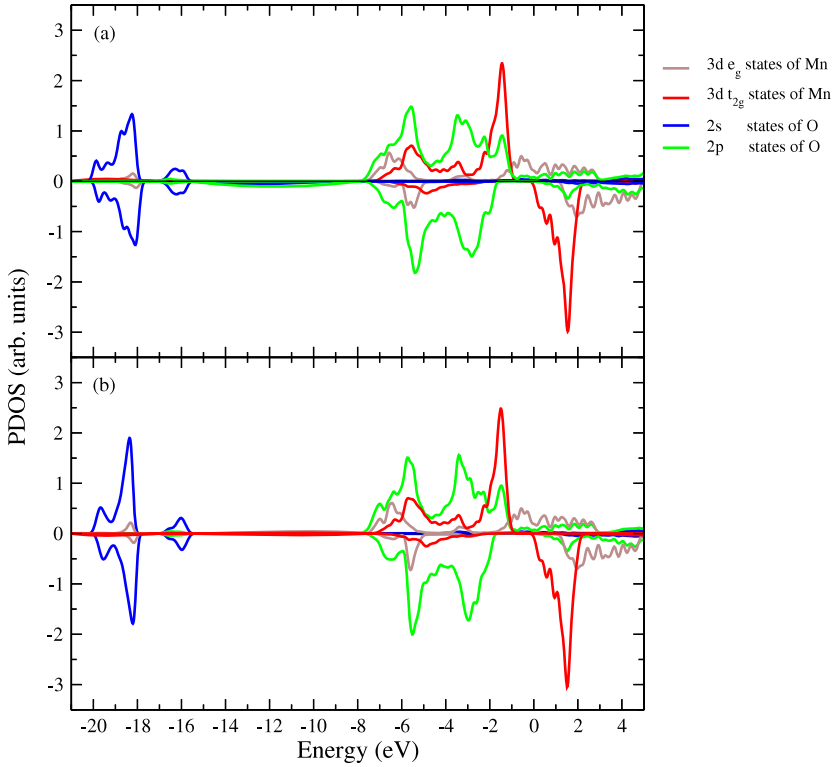


**Figure 6.** The same data as in figure 4, but for structure B.

averaging $\overline{V}(z')$ over a window of width $d$, centered at $z$ [39]:

$$\overline{\overline{V}}(z) = \frac{1}{d}\int_{-d/2}^{d/2} \overline{V}(z+z')\,\mathrm{d}z'$$

where $d$ is the bulk periodicity along [001] (the perovskite $a$ lattice constant in our case).

Inspection of the potential profiles, in figure 5(a), indicates that the values of the macroscopic-averaged electrostatic and local potentials are lower (by 1–2 eV) at the position of the $MnO_2$ La–La-sandwiched plane than at the position of the $MnO_2$ La–Sr-sandwiched plane. This is in agreement with the trend observed in the corresponding Mn and O PDOS[8] and is consistent with the increased positive charge (and hence attractive potential region for electrons) of the La cation with respect to the Sr cation. Based on the gradient of the macroscopic-averaged electrostatic potential, a local electric field is expected in the region of the $MnO_2$ plane sandwiched between the Sr–La layers. This electric field tends to induce a displacement of the O anions towards the La plane and of the Mn cations towards the Sr plane, consistent with the result of the atomic relaxations. Similarly a smaller electric field is also expected in the region of the LaO plane, which should slightly move the O anions in the direction of the $MnO_2$ La–La-sandwiched plane and the La cations in the direction of the $MnO_2$ La–Sr-sandwiched plane. This is also in general agreement with the results of the relaxation calculations.

These ionic relaxations, and the resulting screening of the electric field [40], lead to values of the electrostatic (and local) potential which are very similar at the positions of the La–La-sandwiched and La–Sr-sandwiched $MnO_2$ planes (see figure 5(b)). This in turn shifts in energy the PDOSs of the two $MnO_2$ planes towards each other, as observed in figure 4(b).

The atomic PDOSs and electrostatic potentials of structure B are displayed in figures 6 and 7, respectively, for comparison. The PDOSs of the unrelaxed and relaxed structure B (figure 6) look rather similar and strongly resemble the PDOS of the relaxed structure A (figure 4(b)). This is generally consistent with the constant behavior of the macroscopic-averaged electrostatic potential along [001] in structure B (figure 7). In figure 6, one can notice a slight sharpening with atomic relaxation of some of the features in structure B (the O 2s peaks, in particular). This slight sharpening most likely derives from the screening, induced by the displacements $\Delta y$ of the ions, of the lateral inhomogeneities along [010] in the electrostatic potential.

## 5. Conclusions

LSMO is a material of potential interest for current injection in spintronic devices. In addition to the standard solid solution alloy, it has become recently possible to grow cation-ordered layered phases of $La_{1-x}A_xMnO_3$ materials (with A = Ca or Sr) by epitaxial growth techniques. In this paper we have investigated, by means of *ab initio* calculations, the effects of structural relaxation and Sr-dopant order on the electronic and magnetic properties of LSMO. We compared an LSMO cation-ordered layered structure and an LSMO structure with a more homogeneous distribution of Sr dopants.

[8] One expects the shift in the electronic levels to become closer to that of the electrostatic potential for more strongly localized orbitals.

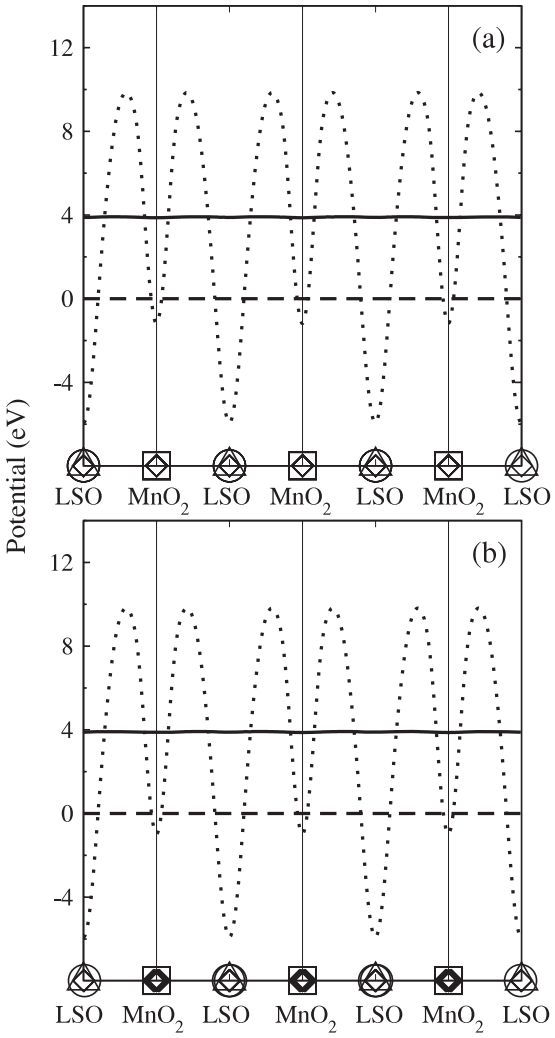


**Figure 7.** The same data as in figure 5, but for the bulk-like LSMO (structure B).

Our results show that both lattice relaxation and an increased homogeneity in the dopant's distribution tend to make LSMO a half-metal, increasing the minority-spin and spin-flip gaps. Within the GGA approach, the relaxed LSMO structure with a homogeneous-like Sr-doping is found to be a half-metal. We have shown that lattice relation—which was neglected in previous studies of the layered structures—has a significant impact on the electronic properties of such systems. Lattice relaxation drastically reduces the initial differences found between the electronic properties of perovskite phases with different dopant ordering. We have explained the trends observed upon lattice relaxation in terms of an effective ionic screening of the local electric field generated by the ordered dopants.

## Acknowledgments

We thank B Davidson and S Nannarone for useful discussions. One of us (BZ) acknowledges support for this work by the Friuli-Venezia-Giulia Regional Government under grant no. 200501611001. Calculations were performed on the IBM SP5 computer at CINECA.

## References

[1] Coey J M D, Viret M and von Molnár S 1999 *Adv. Phys.* **48** 167
[2] Tokura Y (ed) 2000 *Colossal Magnetoresistive Oxides* (*Advances in Condensed Matter Science* vol 2) (Amsterdam: Gordon and Breach)
[3] Ramirez A P 1997 *J. Phys.: Condens. Matter* **9** 8171
[4] Dorr K 2006 *J. Phys. D: Appl. Phys.* **39** R125
[5] Coey J M D and Chien C L 2003 *MRS Bull.* **28** 720
[6] Wolf S A, Awschalom D D, Buhrman R A, Daughton J M, von Molnár S, Roukes M L, Chthelkanova A Y and Treger D M 2001 *Science* **294** 1488
[7] Tsymbal E Y, Mryasov O N and LeClair P R 2003 *J. Phys.: Condens. Matter* **15** R109
[8] Bowen M, Bibes M, Barthelemy A, Contour J P, Anane A, Lemaitre Y and Fert A 2003 *Appl. Phys. Lett.* **82** 233
[9] Nadgorny B 2007 *J. Phys.: Condens. Matter* **19** 315209 and references therein
[10] Krempasky J *et al* 2008 *Phys. Rev.* B **77** 165120 and references therein
[11] Ma C, Yang Z and Picozzi S 2006 *J. Phys.: Condens. Matter* **18** 7717 and references therein
[12] Chikamatsu A *et al* 2006 *Phys. Rev.* B **73** 195105
[13] Yamada H, Ogawa Y, Ishii Y, Sato H, Kawasaki M, Akoh H and Tokura Y 2004 *Science* **305** 646
[14] Horiba K, Chikamatsu A, Kumigashira H, Oshima M, Nakagawa N, Lippmaa M, Ono K, Kawasaki M and Koinuma H 2005 *Phys. Rev.* B **71** 155420
[15] Wang K, Ma Y and Betzler K 2007 *Phys. Rev.* B **76** 144431 and references therein
[16] Picozzi S, Ma C, Yang Z, Bertacco R, Cantoni M, Cattoni A, Petti D, Brivio S and Ciccacci F 2007 *Phys. Rev.* B **75** 094418 and references therein
[17] Pruneda J M, Ferrari V, Rurali R, Littlewood P B, Spaldin N A and Artacho E 2007 *Phys. Rev. Lett.* **99** 226101 and references therein
[18] de Jong M P, Bergenti I, Osikowicz W, Friedlein R, Dediu V A, Taliani C and Salaneck W R 2006 *Phys. Rev.* B **73** 052403 and references therein
[19] Zenia H, Gehring G A and Temmerman W M 2007 *New J. Phys.* **9** 105
[20] Tebano A *et al* 2008 *Phys. Rev. Lett.* **100** 137401
[21] Kumigashira H, Horiba K, Oguchi H, Ono K, Oshima M, Nakagawa N, Lippmaa M, Kawasaki M and Koinuma H 2003 *Appl. Phys. Lett.* **82** 3430
Kumigashira H, Chikamatsu A, Hashimoto R, Oshima M, Ohnishi T, Lippmaa M, Wadati H, Fujimori A, Ono K, Kawasaki M and Koinuma H 2006 *Appl. Phys. Lett.* **88** 192504
[22] Palanisami A, Warusawithana M, Eckstein J N, Weissman M B and Mathur N D 2005 *Phys. Rev.* B **72** 024454
[23] Smadici S, Abbamonte P, Bhattacharya A, Zhai X, Jiang B, Rusydi A, Eckstein J N, Bader S D and Zuo J-M 2007 *Phys. Rev. Lett.* **99** 196404
[24] Geng T and Zhang N 2006 *Phys. Lett.* A **351** 314
[25] Ferrari V, Pruneda J M and Artacho E 2006 *Phys. Status Solidi* a **203** 1437
[26] Livesay E A, West R N, Dugdale S B, Santi G and Jarlborg T 1999 *J. Phys.: Condens. Matter* **11** L279
[27] Pickett W E and Singh D J 1997 *Phys. Rev.* B **55** R8642
Pickett W E and Singh D J 1997 *J. Magn. Magn. Mater.* **172** 237
[28] Pickett W E and Singh D J 1996 *Phys. Rev.* B **53** 1146
[29] Perdew J P, Burke K and Ernzerhof M 1996 *Phys. Rev. Lett.* **77** 3865
[30] Baroni S, de Gironcoli S, Dal Corso A and Giannozzi P *PWSCF (Plane-Wave Self-Consistent Field) codes* http://www.pwscf.org/

[31] Vanderbilt D 1990 *Phys. Rev.* B **41** 7892
[32] King-Smith R D and Vanderbilt D 1994 *Phys. Rev.* B **49** 5828
[33] Zhong W, King-Smith R D and Vanderbilt D 1994 *Phys. Rev. Lett.* **72** 3618
[34] Bellaiche L, Padilla J and Vanderbilt D 1999 *Phys. Rev.* B **59** 1834
[35] Singh D J and Pickett W E 1998 *Phys. Rev.* B **57** 88
[36] Tsui F, Smoak M C, Nath T K and Eom C B 2000 *Appl. Phys. Lett.* **76** 2421
[37] Rajendran V, Kumaran S M, Sivasubramanian V, Jayakumar T and Raj B 2003 *Phys. Status Solidi* a **195** 350
[38] Maurice J L, Pailloux F, Barthelemy A, Durand O, Imhoff D, Lyonnet R, Rocher A and Contour J P 2003 *Phil. Mag.* **83** 3201
[39] Peressi M, Binggeli N and Baldereschi A 1998 *J. Phys. D: Appl. Phys.* **31** 1273
Baroni S, Resta R, Baldereschi A and Peressi M 1989 *Proc. NATO Advanced Research Workshop on Spectroscopy of Semiconductor Microstructures* ed G Fasol *et al* (New York: Plenum) p 251
[40] Binggeli N, Ferrara P and Baldereschi A 2001 *Phys. Rev.* B **63** 245306